Available online at www.sciencedirect.com
ScienceDirect
Geochimica et Cosmochimica Acta 74 (2010) 1294–1308
Geochimica et Cosmochimica Acta
www.elsevier.com/locate/gca

Germanium–silicon fractionation in a tropical, granitic weathering environment

Festo Lugolobi [a], Andrew C. Kurtz [a,*], Louis A. Derry [b]

[a] Department of Earth Sciences, Boston University, Boston, MA 02215, USA
[b] Department of Earth and Atmospheric Sciences, Cornell University, Ithaca, NY 14853, USA

Received 29 April 2009; accepted in revised form 17 November 2009; available online 27 November 2009

Abstract

Germanium–silicon (Ge/Si) ratios were determined on quartz diorite bedrock, saprolite, soil, primary and secondary minerals, phytolith, soil and saprolite pore waters, and spring water and stream waters in an effort to understand Ge/Si fractionation during weathering of quartz diorite in the Rio Icacos watershed, Puerto Rico. The Ge/Si ratio of the bedrock is 2 μmol/mol, with individual primary mineral phases ranging between 0.5 and 7 μmol/mol. The ratios in the bulk saprolite are higher (~3 μmol/mol) than values measured in the bedrock. The major saprolite secondary mineral, kaolinite, has Ge/Si ratios ranging between 4.8 and 6.1 μmol/mol. The high Ge/Si ratios in the saprolite are consistent with preferential incorporation of Ge during the precipitation of kaolinite. Bulk shallow soils have lower ratios (1.1–1.6 μmol/mol) primarily due to the residual accumulation of Ge-poor quartz.

Ge/Si ratios measured on saprolite and soil pore waters reflect reactions that take place during mineral transformations at discrete depths. Spring water and baseflow stream waters have the lowest Ge/Si ratios (0.27–0.47 μmol/mol), reflecting deep initial weathering reactions resulting in the precipitation of Ge-enriched kaolinite at the saprolite–bedrock interface. Mass-balance calculations on saprolite require significant loss of Si and Al even within 1 m above the saprolite–bedrock interface. Higher pore water Ge/Si ratios (~1.2 μmol/mol) are consistent with partial dissolution of this Ge-enriched kaolinite. Pore water Ge/Si ratios increase up through the saprolite and into the overlying soil, but never reach the high values predicted by mass balance, perhaps reflecting the influence of phytolith recycling in the shallow soil.

1. INTRODUCTION

Chemical weathering is a fundamental process at the earth's surface that impacts a wide range of disciplines, from geochemistry to hydrology to biology to paleoclimatology. As a result many geochemical techniques have been developed to study this process. Field-based studies of chemical weathering typically involve elemental/ionic mass balance (Garrels and Mackenzie, 1967; McDowell and Asbury, 1994; Stonestrom et al., 1998; White et al., 1998; Gaillardet et al., 1999; Anderson et al., 2002; Turner et al., 2003) and/or tracers such as strontium isotopes (Blum et al., 1993; Capo et al., 1998; Derry et al., 2006; Pett-Ridge et al., 2009), silicon isotopes (e.g., Ziegler et al., 2005), or germanium–silicon ratios (Murnane and Stallard, 1990; Froelich et al., 1992; Kurtz et al., 2002; Derry et al., 2005), or soil chemistry and mineralogy (e.g., Vitousek et al., 1997; Chadwick et al., 1999). All of these approaches have their benefits and limitations. In this study we further the development of germanium–silicon ratios as a tracer of chemical weathering processes and the biogeochemical cycle of silicon. Understanding silicate weathering is important in terms of soil development, availability of nutrients in soils, buffering acid rain and is a long-term sink for atmospheric CO_2.

Germanium is a trace element in the earth's crust with an average concentration of <2 ppm (e.g., Bernstein, 1985). Ge

* Corresponding author. Address: Department of Earth Sciences, Boston University, 675 Commonwealth Ave., Boston, MA 02215, USA. Tel.: +1 617 358 2570.
E-mail address: kurtz@bu.edu (A.C. Kurtz).

0016-7037/$ - see front matter © 2009 Elsevier Ltd. All rights reserved.
doi:10.1016/j.gca.2009.11.027

and Si have very similar chemical properties due to similar ionic radii (Si; 2.6 Å, Ge: 3.9 Å), and electronic configuration. Ge tends to substitute for Si in silicate minerals (e.g., Goldschmidt, 1926, 1958; Lewis et al., 1988; Martin et al., 1996), largely because both elements have similar tetrahedral bond length, 1.75 Å for Ge–O, and 1.64 Å for Si–O (Shannon and Prewitt, 1969; Shannon, 1976). The result of such substitutions is that primary (igneous) silicate minerals tend to have characteristic Ge/Si ratios averaging between 1 and 3 μmol/mol (DeArgollo and Schilling, 1978; Bernstein, 1985). Incorporation of Ge into the silicate lattice appears to vary with the degree of linkage in the crystallographic structure, such that sheet and chain silicates (biotite, amphibole) tend to have higher Ge/Si ratios than tectosilicates (quartz, feldspar) (e.g., Bernstein, 1985).

Soils tend to have Ge/Si ratios higher than the parent material from which they are derived (Murnane and Stallard, 1990; Kurtz et al., 2002; Scribner et al., 2006). This weathering fractionation may largely reflect preferential incorporation of Ge by neoformed (sheet-silicate) clay minerals, but refractory non-silicate minerals also appear to sequester Ge in some soils (Scribner et al., 2006). The only comprehensive studies of Ge/Si fractionation in the weathering environment to date were done on soils derived from fine-grained to glassy basaltic parent material in Hawaii (Kurtz et al., 2002; Scribner et al., 2006). Limited Ge/Si data on granitic soils presented by Kurtz et al. (2002) indicate that Ge/Si fractionation in granitoid landscapes may differ significantly due to differential weathering rates of individual mineral phases.

Ge/Si ratios in rivers and streams tend to be lower than bedrock ratios, again reflecting the partitioning of Ge into secondary minerals in soil during chemical weathering (Mortlock and Froelich, 1987; Murnane and Stallard, 1990; Anders et al., 2003). Murnane and Stallard (1990) postulated that Ge/Si ratios in streams can be explained by a mixture between Si derived from the incongruent weathering of primary minerals (high Si, low Ge/Si solution) and dissolution of Ge-enriched secondary minerals (low Si, high Ge/Si solution). Stream Ge/Si ratios would therefore reflect weathering intensity integrated over the watershed scale. However, a more recent study by Derry et al. (2005) attributed very high Si, low Ge/Si stream waters in Hawaii to biological cycling of Si and dissolution of plant-derived opal phytoliths in Hawaiian soils. One outstanding question is to what extent do stream water Ge/Si ratios in general reflect silicate weathering vs. the importance of biological cycling?

In this paper, we present Ge/Si data on soil, saprolite, primary and secondary minerals, phytoliths, soil and saprolite pore waters, spring water and stream water from the Rio Icacos site in eastern Puerto Rico. Together these data provide a comprehensive study of Ge/Si fractionation in granitic soil from the perspective of mineral transformations and the solutions they produce during silicate weathering.

2. STUDY SITE

Our study site is located in the Luquillo Experimental Forest (within the Caribbean National Forest in eastern Puerto Rico), in the Rio Icacos watershed (Fig. 1). This area has been investigated as part of three major research programs, as a site in the Long Term Ecological Research (LTER) network, a USGS "Water Energy and Biogeochemical Budgets" (WEBB) site, and it has recently become an observatory in the emerging Critical Zone Exploration Network (CZEN). As a result, there has been extensive prior site characterization, making this site an excellent candidate for testing of new tracers of weathering and biogeochemical cycling.

Rio Icacos and its tributary the Rio Guaba cover an area of 326 ha, underlain by a medium to coarse-grained 40 Ma Rio Blanco quartz diorite (Seiders, 1971; White et al., 1998). Major mineral constituents of the quartz diorite in order of decreasing abundance include plagioclase, quartz, biotite, hornblende and goethite (White et al., 1998). Soils are generally less than 1 m in thickness with a thin (~0.1 m) A/B horizon, and a kaolinite-rich B horizon (e.g., Boccheciamp, 1977; White et al., 1998). This intensely weathered soil overlies a partially oxidized saprolite which can be as thick as 8 m on ridge tops, and as thin as 1 m in some parts of the hill slopes. At the base of the saprolite there is an abrupt transition through oxidized saprock to a competent but fractured bedrock (e.g., Buss et al., 2008).

Kaolinite is the most abundant secondary mineral in the saprolite and soils and it is present in two types that reflect their formation mechanisms (Dong et al., 1998; Murphy et al., 1998). Type I kaolinite is fine-grained (<2 μm) and is thought to be formed through dissolution–precipitation (neoformation) processes involving mainly plagioclase (Dong et al., 1998; Murphy et al., 1998). Type II kaolinite forms through pseudomorphosis of primary biotite throughout the saprolite, increasing in abundance up through the saprolite (e.g., Dong et al., 1998; Murphy et al., 1998). Other minerals in the saprolite and soil include quartz, biotite and hornblende.

Dominant plants species include Tabonuco (*Dacryodes excelsa*), Colorado (*Cyrilla racemiflora*), *Cecropia peltata*, Sierra palms and ferns (Brown et al., 1983; McDowell and Asbury, 1994). This site receives over 420 cm of rainfall per year and has an annual average temperature of 22 °C (McDowell and Asbury, 1994). These climate conditions in conjunction with steep slopes (45°) may account for the world's fastest measured rates of granitoid weathering (McDowell and Asbury, 1994; White et al., 1998).

3. METHODS

3.1. Sample collection and processing

3.1.1. Rock and mineral samples

To understand Ge/Si fractionation during chemical weathering and Si cycling in the Rio Icacos watershed we employed studies of all major Si reservoirs; rock, soil, plant phytoliths and water samples. A fresh sample of unweathered diorite was obtained from a road cut near the Guaba stream gauging station. It was crushed and mineral separates of biotite and hornblende were isolated by handpicking. A staining procedure was used to differentiate quartz from plagioclase, which would be otherwise extremely diffi-

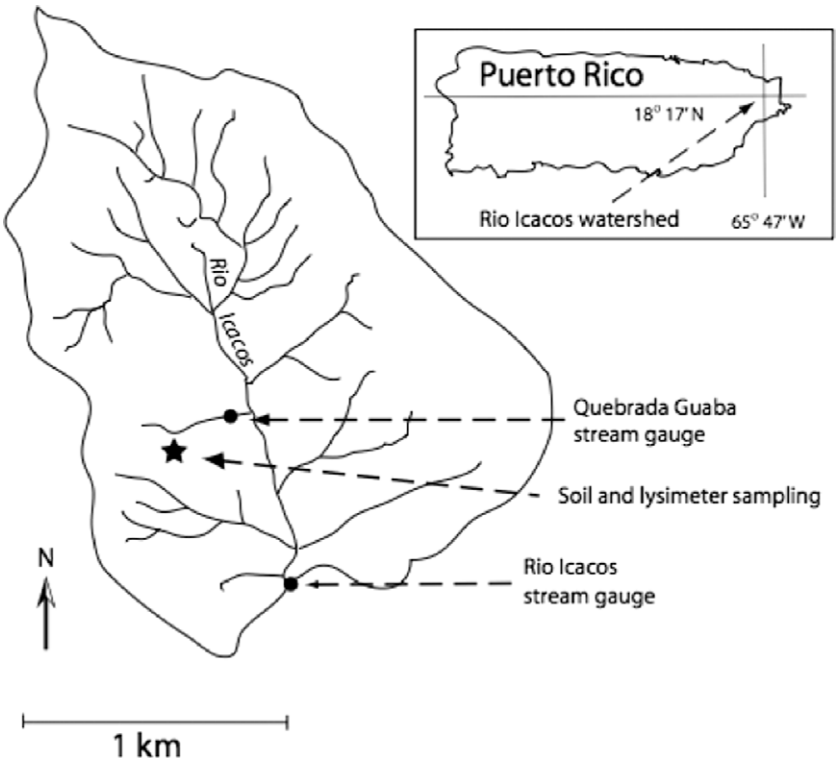

Fig. 1. Map showing location of Rio Icacos watershed in Puerto Rico, and location of study site within the watershed. Sites LG1, LG2, and LG3 established by White et al. (1998) are located within the star symbol. Figure from Pett-Ridge et al. (2009).

cult to handpick. A sieved coarse-fraction mixture of largely quartz and plagioclase was etched with hydrofluoric acid, rinsed, and immersed in Amaranth solution to stain the plagioclase with a red color. Separated mineral grains and whole rock samples were powdered using a boron carbide mortar and pestle and prepared for analysis following the same procedure described below for soil samples. Purity of the plagioclase separate was verified using X-ray diffraction and checked with chemical composition. Our plagioclase separate yielded a Si/Al molar ratio of 1.94 identical to the value obtained using a microprobe by White et al. (1998).

3.1.2. Soil and saprolite samples

Prior work by White et al. (1998) established a group of study sites (LG1, LG2 and LG3) on a ridge top, 200 m uphill from the Rio Guaba stream gauging station (Fig. 1). Soil and saprolite samples used for this study were provided by Pett-Ridge (Oxford), obtained by hand-auguring to the bedrock at ~8 m, immediately adjacent to the LG1 site. Splits of soil (0–60 cm) and saprolite (75–735 cm) samples were dried overnight at 105 °C then heated at 550 °C for 4 h to remove organic matter and other volatiles including structurally bound water in clay minerals. The change in weight at this step is recorded as "loss on ignition" (LOI, wt%). Samples were then pulverized using a boron carbide mortar and pestle and stored in a desiccator prior to further analyses. The powered samples were dissolved using the lithium tetraborate fusion method. One hundred milligrams (100 mg) of soil were weighed into a graphite crucible, mixed with 400 mg of lithium tetraborate and fused in a muffle furnace at 1050 °C for 15 min. The partially melted bead was removed from the furnace, swirled to ensure uniform mixing of sample and flux and reheated for another 5 min. The melted sample was then dissolved in 50 ml of 10% nitric acid and sonicated for 30 min to ensure complete dissolution of the sample. The solution was then filtered and diluted to 4000-fold dilution with deionized water prior to analysis.

Kaolinite was separated from the saprolite by first treating ~10 g of bulk saprolite sample with hydrogen peroxide to remove organic matter. The organic free sediment underwent a settling procedure to separate out the clay fraction (e.g., Day, 1965). X-ray diffraction showed that the clay fraction was quartz-free. Residual iron-oxyhydroxides were likely present in the kaolinite separates as indicated by Fe_2O_3 concentrations reported in Table 1. The presence of such iron-oxyhydroxides should not have a significant impact on measured Ge/Si ratios (Scribner et al., 2006). The separated kaolinite was dissolved following the procedure described above and analyzed for major elements and Ge concentrations.

3.1.3. Water samples

Tension lysimeters (PVC tubes with porous ceramic cups) were previously installed by USGS researchers (White et al., 1998) at sites designated LG1, LG2 and LG3, at depths ranging from 15 cm to 850 cm. We sampled these lysimeters during the field campaigns on July 13, 2003 and February 14, 2004. Lysimeters were emptied and reset

Table 1
Elemental concentrations and Ge/Si ratios in the Luquillo diorite, primary and secondary minerals.

	SiO_2 (wt%)	Al_2O_3 (wt%)	Fe_2O_3 (wt%)	CaO (wt%)	K_2O (wt%)	MgO (wt%)	MnO (wt%)	Na_2O (wt%)	TiO_2 (wt%)	P_2O_5 (wt%)	Ge (ppm)	Zr (ppm)	Ge/Si (μmol/mol)
Diorite	61.8	17.7	5.1	6.12	1.04	1.79	0.12	3.53	0.37	0.10	1.49	56	2.0
Diorite minerals													
Quartz[a]	99.2	0.3	nd	nd	nd	nd	nd	nd	nd	nd	0.6		0.5
Feldspar	58.6	25.0	0.20	8.54	0.71	0.14	0.01	5.37	0.04	0.06	1.06		1.5
Biotite	39.5	15.2	21.1	2.36	7.62	9.98	0.43	0.56	2.50	0.18	2.5		5.2
Hornblende	46.4	9.4	21.8	7.10	2.54	9.59	0.60	0.85	1.47	0.28	3.9		7.0
Saprolite minerals													
Kaolinite-I (9 cm)	41.4	16.0	4.92	nd	0.05	0.25	0.01	0.25	0.61	0.47	2.47		4.9
Kaolinite-I (714 cm)	34.2	33.3	13.1	nd	0.12	0.33	1.46	0.27	0.84	0.62	2.51		6.1
Kaolinite-II (714 cm)	49.4	25.0	8.15	nd	1.54	2.33	0.37	0.04	1.05	0.07	2.88		4.8

[a] Quartz data from Kurtz et al., 2002; nd = concentration below limit of quantification.

to a suction of −60 kPa the day prior to sampling. Groundwater flowing at the saprolite–bedrock interface was collected at a spring emanating from a nearby landslide scar, 200 m east of the Guaba stream gage. We also collected baseflow samples from the Icacos and Guaba streams. All water samples were filtered through a 0.45 μm filter, acidified with 2–3 drops of concentrated nitric acid and refrigerated prior to analysis.

3.1.4. Soil paste experiments

In addition to pore waters sampling by tension lysimeters, we performed saturation paste experiments using soil samples from the LG1 site, following the same procedure used by Derry et al. (2005) in their Ge/Si study in Hawaii. These experiments both supplement the lysimeter sampling of soil solutions, and allow for a more direct comparison with the data of Derry et al. (2005). These experiments provide more detailed information on soil solutions from the top 50 cm of the soil profile, where we might expect to find the elevated Si concentrations and low Ge/Si ratios that indicate the influence of phytoliths (e.g., Derry et al., 2005; Blecker et al., 2007). A 70 cm soil core was collected using a hammer-assisted push corer. The core was sliced in 4 cm intervals using a plastic knife. One hundred grams (100 g) of well homogenized soil from each depth interval was transferred into 250 ml polypropylene beakers and mixed with distilled water to field capacity and left to sit for 1 h (e.g., Lathja et al., 1999). After leaching, the soil slurries were filtered through a 0.45 μm filter. The filtrate transferred into 30 ml plastic bottles, acidified and analyzed for major cations and Ge following the methods described below. Concentrations of elements in these soil solutions are not in any way normalized to the mass of soil used in the experiment.

3.1.5. Plant phytolith extractions

We collected whole leaf samples from eight species found adjacent to the LG1 site to determine the phytolith content (as wt% SiO_2) in leaves and the Ge/Si ratios in phytoliths. The leaves were cleaned with distilled water and left to dry overnight at 50 °C. Leaves were then crushed in a mortar and pestle with liquid nitrogen and 0.5 g weighed into a Teflon microwave vessel. Nine milliliters of 70% nitric acid and hydrogen peroxide (1 ml) were added to the vessel. Care was taken to make sure that the entire leaf sample was covered with the acid–peroxide mixture. The samples were left to sit uncovered for 10 min to allow initial oxidation by the peroxide. The samples were capped and heated in the Milestone Ethos II microwave at 180 °C for 10 min. The microwave vessels were allowed to cool for 1 h and each sample was transferred to a 50 ml tube, centrifuged and the acid decanted from the solid phytolith sample, which was then washed five times with deionized water. The concentration of Si in the supernatant was found to be near detection limit, indicating minimal dissolution of phytoliths. Clean phytolith samples were dissolved in 5 ml of 2 M sodium hydroxide and diluted 5-fold with deionized water. Because of the high sodium hydroxide content, the samples were neutralized to pH 3 with nitric acid prior to analysis.

3.2. Sample analyses

All analyses for both major elements and Ge were performed in the analytical laboratories at Boston University. Major element analyses were performed using the Jobin Yvon Ultrace JY-138 Inductively Coupled Plasma-Emission Spectrometer (ICP-ES). Five standard reference materials (BHVO2, G-2, RGM-1, SCO-1 and STM) were used during major element analyses of rock, saprolite and soil samples. For water sample analyses we used multi-element standard solutions at concentrations that bracketed the concentrations of our water samples prepared from stock single element standard solutions (Fisher Scientific). A representative sample with major elements concentration similar to our samples was run with the samples to track and correct for instrumental drift. Major element analyses of SRM BHVO2 run as an unknown agree to accepted values to within 2%, with 2 sigma precision better than 3% based on replicate analyses. Two sigma precision on dissolved Si

concentrations is 1.2% based on four replicate analyses of a single water sample.

Samples for Ge analysis were prepared by mixing 10 g of the sample (water or diluted dissolved solid) with a ^{70}Ge-enriched spike ($^{70}Ge/^{74}Ge = 161$) to a target $^{70}Ge/^{74}Ge$ ratio of ~3. The samples and spike were allowed to equilibrate at room temperature for at least 24 h. For rock and saprolite samples we a used continuous hydride generation method (Scribner et al., 2006). Here, the spiked sample was mixed inline with a 0.2 M Tris–HCl solution followed by a 2% sodium borohydride solution, and the generated hydride swept into the torch of the ICP-MS in an argon gas stream. Because water samples contained lower Ge concentrations, we used a cryogenic "batch" method to concentrate the generated GeH_4. During this procedure the equilibrated solution was buffered to pH 6 by 0.5 ml of a 2 M Tris–HCl solution. The sample was then connected to the hydride line and using a syringe 0.5 ml of 4% sodium borohydride was added to the samples to generate germanium hydride (GeH_4). The generated germanium hydride was collected for 4 min and trapped in a U-tube immersed in liquid argon before introducing it as a plug into the torch of the VG Plasmaquad 2+ ICP-MS (Jin et al., 1991; Mortlock and Froelich, 1996; Kurtz et al., 2002; Derry et al., 2005). Replicate analyses of Ge concentrations in water samples agree to within 4%. Our analysis of Ge in SRM SCO-1 (1.45 ppm) agrees within error to the value published by Scribner et al. (2006; 1.44 ± 0.01).

4. RESULTS

4.1. Quartz diorite parent material

The quartz diorite parent material contains 1.49 ppm Ge, reflecting a mixture of minerals with Ge concentrations ranging from 0.6 ppm (quartz) to 3.9 ppm (hornblende; Table 1). With a SiO_2 concentration of 61.8 wt%, the bulk rock Ge/Si ratio is 2.0 μmol/mol. Individual mineral Ge/Si ratios range from 0.5 to 7.0 μmol/mol. The dominant mineral phase, plagioclase, has a Ge concentration of 1.06 ppm and a Ge/Si ratio of 1.5 μmol/mol.

Table 2
Elemental concentrations[a] and Ge/Si ratios with depth in the Luquillo weathering profile

	Depth (cm)	SiO_2 (wt%)	Al_2O_3 (wt%)	Fe_2O_3 (wt%)	CaO (wt%)	K_2O (wt%)	MgO (wt%)	MnO (wt%)	Na_2O (wt%)	TiO_2 (wt%)	Sr (ppm)	Zr (ppm)	Ge (ppm)	Ge/Si (μmol/mol)	LOI (wt%)
Soil	15	78.3	12.6	3.89	nd	0.31	0.15	0.02	nd	0.35	4.51	187	1.40	1.5	8.90
	45	83.4	11.1	4.42	nd	0.21	0.10	0.02	nd	0.33	2.04	147	1.11	1.1	7.32
	60	69.5	15.6	5.67	nd	0.45	0.32	0.04	nd	0.4	2.51	142	1.33	1.6	8.34
Saprolite	75	65.4	21.4	6.54	nd	0.84	0.65	0.10	nd	0.48	3.61	118	1.57	2.0	8.07
	120	69.1	22.7	7.09	nd	0.89	0.67	0.13	nd	0.51	10.66	121	2.04	2.4	7.97
	150	68.7	20.7	7.33	nd	0.97	0.76	0.13	nd	0.51	4.62	130	2.39	2.9	7.26
	180	66.6	23.5	7.79	nd	1.10	0.69	0.07	nd	0.57	3.79	128	2.14	2.7	8.03
	210	64.4	22.4	7.53	nd	1.12	0.74	0.09	nd	0.51	3.28	109	2.08	2.7	8.09
	240	69.0	22.2	8.27	nd	1.33	0.76	0.11	nd	0.57	9.39	141	2.02	2.4	7.75
	270	69.4	21.4	7.46	nd	1.05	0.70	0.14	nd	0.55	3.2	113	1.93	2.3	7.54
	300	65.5	23.2	8.41	nd	1.05	0.67	0.11	nd	0.6	5.44	149	1.95	2.5	8.33
	330	67.7	21.8	7.47	nd	1.16	0.74	0.13	nd	0.53	4.3	172	1.50	1.8	7.61
	360	69.9	22.1	6.39	nd	0.82	0.58	0.37	nd	0.46	3.62	161	2.20	2.6	7.95
	390	69.7	22.0	7.18	nd	1.15	0.70	0.19	nd	0.53	3.72	117	1.94	2.3	8.12
	420	66.7	21.5	7.27	nd	1.21	0.69	0.55	nd	0.52	4.01	137	2.40	3.0	7.89
	450	66.4	22.6	7.86	nd	1.07	0.66	0.25	nd	0.58	3.62	111	2.27	2.8	8.00
	480	65.4	21.1	7.27	0.69	1.65	1.40	0.24	0.53	0.57	24.9	180	2.08	2.6	7.27
	495	68.8	19.4	7.04	0.74	1.34	1.12	0.27	0.56	0.49	27.9	88.1	1.74	2.1	6.75
	510	65.8	19.3	6.61	1.77	1.42	1.56	0.21	1.18	0.49	57.7	85.6	1.77	2.2	5.84
	525	65.1	19.9	7.25	1.69	1.36	1.70	0.20	1.0	0.53	49.2	144	1.72	2.2	6.51
	540	65.6	18.3	6.68	2.48	1.45	1.91	0.43	1.54	0.48	73.0	83.8	1.59	2.0	4.75
	555	66.5	19.6	7.13	2.56	1.58	1.93	0.33	1.59	0.54	81.0	97.0	1.56	1.9	4.88
	570	59.4	16.5	6.81	3.58	1.50	2.10	0.18	2.15	0.48	117	86.4	1.60	2.2	3.07
	585	66.4	17.1	6.76	3.7	1.64	2.15	0.18	2.26	0.49	121	97.6	1.63	2.0	3.09
	600	63.9	17.2	6.36	3.89	1.70	2.06	0.18	2.52	0.47	133	67.0	1.50	1.9	2.84
	630	63.9	18.4	6.68	4.04	1.68	2.19	0.20	2.47	0.51	135	88.6	1.69	2.2	3.12
	645	65.9	17.5	6.91	4.22	1.76	2.14	0.18	2.68	0.52	148	110	1.45	1.8	2.36
	660	67.9	17.9	6.53	4.02	1.76	2.06	0.17	2.38	0.49	142	84.6	1.60	2.0	2.96
	675	65.2	17.4	7.23	4.37	1.86	2.40	0.20	2.64	0.53	144	113	1.61	2.0	2.52
	690	63.9	17.5	7.06	4.34	1.85	2.36	0.21	2.61	0.53	145	69.5	1.68	2.2	2.41
	705	63.4	16.8	6.67	4.25	1.70	2.17	0.19	2.62	0.48	145	68.3	1.50	2.0	2.23
	720	65.5	17.8	7.43	4.69	1.74	2.55	0.23	2.82	0.53	152	104	1.75	2.2	2.29
	735	65.4	17.9	7.15	4.59	1.87	2.46	0.22	2.8	0.53	152	93.4	1.70	2.2	2.39

nd = concentration below limit of quantification

[a] Concentrations are based on "volatile-free" sample weight, after to heating to 550 °C. LOI is reported for reference.

4.2. Saprolite and soil

Elemental concentrations measured on a core from the LG1 site are presented in Table 2. These concentrations are reported and discussed based on their "volatile-free" (after heating to 550 °C) weight to allow discrimination of vertical trends in soil and saprolite elemental composition reflecting weathering without dilution effects from variable LOI, which increases sharply between 6 and 5 m depth (Table 2). Results are discussed here moving up from the saprolite–bedrock interface toward the surface, reflecting increasing duration of weathering upward. SiO_2 concentrations in the saprolite are generally elevated relative to bedrock resulting from residual concentration by loss of more mobile elements. SiO_2 concentrations increase slightly upward from ~65% near the bedrock to values close to 68% at the top of the saprolite (Fig. 2a). More significant depth trends are seen in Ca (Fig. 2b) and Al (Fig. 2c). CaO concentrations are ~4.5 wt% near the saprolite–bedrock interface, decrease slightly upward, and then fall off sharply essentially to zero between 6 and 5 m depth. Al_2O_3 concentrations at depth in the saprolite are similar to bedrock concentrations (~17.7 wt%), then increase to concentrations between 20% and 23% above 5 m. Saprolite Ge concentrations average ~1.6 ppm from saprolite–bedrock interface up to 5 m depth and increase above 5 m to a new average of ~2 ppm that persists upward throughout the saprolite (Table 2). Ge/Si ratios are generally higher in saprolite than in parent material. The Ge/Si ratio measured from our deepest sample, closest to saprolite–bedrock interface is 2.15 μmol/mol. The ratio fluctuates around 2 μmol/mol up to 5 m depth. Above 5 m, Ge/Si ratios increase sharply to values close to 3 μmol/mol and remain high throughout the mid-saprolite up to 1.5 m depth (Fig. 3).

There is an abrupt change in chemistry within the top meter of the weathering profile, where saprolite gives way to chemically and texturally distinct soil (above 60 cm).

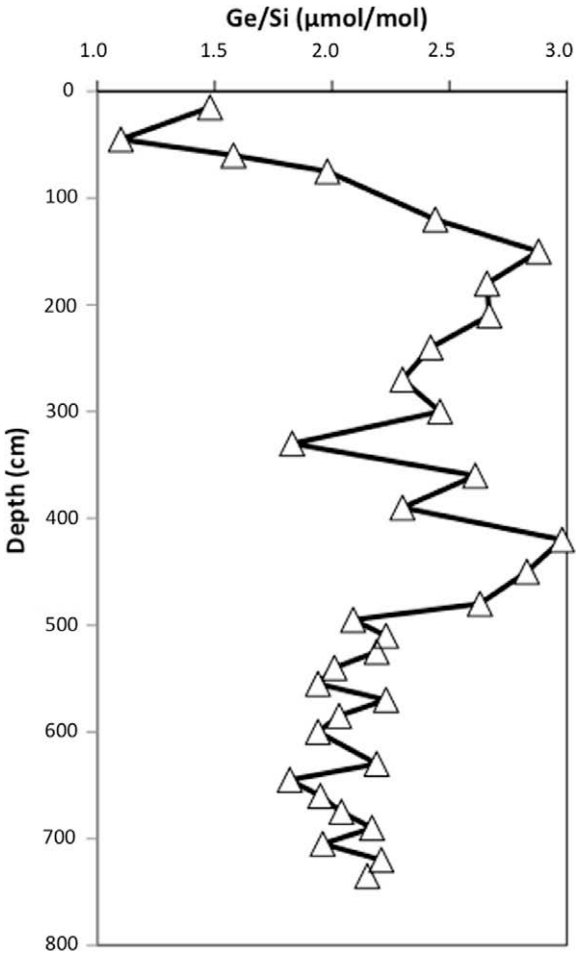

Fig. 3. Depth-profile for solid-phase Ge/Si in soil/saprolite core from LG1 site. Drop in Ge/Si in upper soils likely reflects partial loss of kaolinite produced lower in weathering profile.

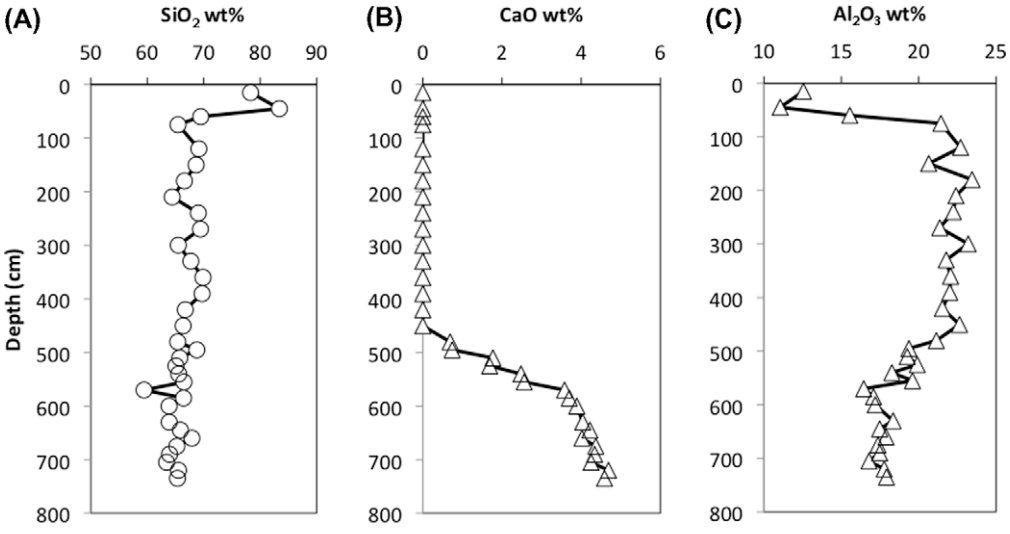

Fig. 2. Depth-profiles for solid-phase (a) SiO_2, (b) CaO and (c) Al_2O_3 in soil/saprolite core from LG1 site. Abrupt loss of CaO at ~5 m depth represents final depletion of primary plagioclase.

Our sampling resolution does not allow discrimination of soil composition by horizon. SiO_2 concentrations increase within the soil reaching values as high as 83% near the surface (Fig. 2b). The increase in Si is complemented by an abrupt decrease in Al concentrations in soil, to Al_2O_3 concentrations ~11–16%. Similarly, Ge concentrations decrease in soil relative to underlying saprolite, to values <1.5 ppm. Increasing Si combined with decreasing Ge causes Ge/Si ratios to decrease to as low as 1.1 μmol/mol in shallow soils (Fig. 3).

The dominant minerals in saprolite and soil, quartz and kaolinite, have distinctive Ge/Si ratios. Quartz has the lowest Ge/Si ratio of any primary or secondary mineral (0.5 μmol/mol). The two types of kaolinite present within the regolith have similarly high Ge/Si ratios. The Ge/Si ratios of two samples of kaolinite derived from dissolution of primary minerals near the saprolite–bedrock interface (type I kaolinite) are 4.9 and 6.1 μmol/mol. Our sample of type II kaolinite, the form derived from pseudomorphosis of biotite, has Ge/Si of 4.8 μmol/mol (Table 1).

4.3. Phytoliths

Leaf phytolith contents (as wt% SiO_2) and Ge/Si ratios in extracted phytoliths from eight plant species at our study site are reported in Table 3. Leaves from the Rio Icacos site contain between 0 and 4.4 wt% SiO_2. We found no systematic relationship between phytolith content and plant type (trees vs. ferns vs. grasses), but our sampling design was aimed at characterizing Ge/Si ratios rather than accurately assessing biomass phytolith content. Ge/Si ratios measured on extracted phytoliths range between 0.03 and 0.5 μmol/mol, by far the lowest ratios in any solid-phase materials at Rio Icacos. There is no clear relationship between phytolith abundance (wt% SiO_2) and Ge/Si ratio in our samples.

4.4. Water samples

Si, Ge and major cation concentrations in waters from tension lysimeters, streams, and saturation paste experiments are reported in Table 4. We report solution data in molality units (mol/kg water) consistent with our gravimetric production of standard solutions. Soil pore water Si concentrations are generally greater than 100 μmol/kg in our deepest lysimeters, and lower than 100 μmol/kg above 5.5 m depth. Concentrations decrease up-profile within the saprolite to a minimum of 30 μmol/kg around 150–60 cm depth (Fig. 4). Dissolved Si concentrations increase above this depth, but do not exceed the highest concentrations measured from the deepest part of the saprolite. Stream waters at baseflow have Si concentrations that are 258–326 μmol/kg. Water samples collected from springs emanating from the saprolite–bedrock interface at nearby landslide areas have Si concentrations (324–349 μmol/kg) that are very similar to or slightly higher than values measured on baseflow stream waters (Table 4).

Germanium pore water concentrations are generally between 100 and 250 pmol/kg (Table 4) and do not show systematic depth trends to the degree that Si concentrations do. The lowest saprolite pore water Ge/Si ratios, ~1.2 μmol/mol were observed 1 m above the saprolite–bedrock interface at LG1 (Fig. 5). Saprolite pore water Ge/Si ratios above 5.5 m are generally between 2 and 3.5 μmol/mol. The highest pore water Ge/Si ratios are seen in the soil (top 60 cm) of LG1 and LG2, where we measure ratios as high as 4.1 μmol/mol. Ge/Si ratios measured on baseflow stream samples and springs are lower than any measured within the weathering profile, ranging from 0.27 to 0.47 μmol/mol.

4.4.1. Soil paste experiments

Results from soil paste experiments from the shallow soil core collected at the LG1 site (Table 4) show that soils release Si to water rapidly (within 1 h in our experiments), producing Si concentrations that are similar to values measured on lysimeter samples from equivalent depths. Interestingly, there is a trend towards higher Si concentrations in the soil solutions extracted from the shallowest samples. Si is only 32 μmol/kg at 55 cm, and increases to 138 μmol/kg in the 2 cm depth sample. Ge concentrations range between 61 and 233 pmol/kg (Table 4), within the range of Ge concentrations measured from the same depths in lysimeter samples. Ge/Si ratios of extracted soil solutions average ~1.85 μmol/mol, slightly lower than lysimeter samples from equivalent depths.

Table 3
Phytolith content (as wt% SiO_2) and Ge/Si ratios in common Luquillo plants.

	SiO_2 (wt%)	Ge/Si (μmol/mol)
Sawgrass	2.9	0.53
Sierra palm (*P. montana*)	3.0	0.12
Melastomataceae	0.02	nd
Cecropia	4.4	0.03
Grass	0.6	0.21
Common fern	4.3	0.2
Fire fern (Gleicheniaceae)	1.7	0.11
Tree fern (*C. arborea*)	0.3	0.17

nd = Ge concentration below limit of quantification.

5. DISCUSSION

Weathering processes have been extensively studied in Luquillo Experimental Forest using a number of techniques (e.g., White et al., 1998; Murphy et al., 1998; Turner et al., 2003; Ziegler et al., 2005; Pett-Ridge et al., 2009). Our aim here is to show how Ge/Si ratios measured on the diorite, saprolite, individual minerals, phytoliths, and water samples can trace particular weathering reactions taking place within the subsurface and also discriminate sources of Si to surface waters.

5.1. Ge/Si fractionation by weathering

Ge/Si ratios of bulk saprolite and soil reflect the sum of the remaining primary minerals plus fractionations that have taken place in the formation of secondary minerals. The Ge/Si ratio of bulk saprolite can differ from parent material either due to incongruent weathering reactions that preferentially take up Ge, or because the saprolite has preferentially retained primary minerals with unusually

Table 4
Dissolved element concentrations and Ge/Si ratios of soil pore waters, saturation paste experiment, stream waters, and spring waters.

	Depth (cm)	Sampling date	Si (μmol/kg)	Ca (μmol/kg)	K (μmol/kg)	Mg (μmol/kg)	Na (μmol/kg)	Ge (pmol/kg)	Ge/Si (μmol/mol)
Pore water									
LG1 site									
LG1-S11	15	Jun-03	60	3.7	3.6	45	236	246	4.1
LG1-S6	31	Jun-03	73	1.2	1.3	27	129	176	2.4
LG1-S4	61	Jun-03	59	1.5	6.4	29	160	138	2.4
LG1-S10	91	Jun-03	40	6.5	7.7	31	206	126	3.1
LG1-S7	152	Jun-03	54	0.7	0.8	14	90	132	2.5
LG1-S1	183	Jun-03	51	3.5	8.7	37	203	133	2.6
LG1-S12	244	Jun-03	72	2.0	6.1	17	84	212	2.9
LG1-S3	366	Jun-03	89	6.0	8.4	23	173	202	2.3
LG1-S9	548	Jun-03	78	6.2	10.2	19	92	204	2.6
LG1-S5	671	Jun-03	176	5.5	21.5	38	130	188	1.1
LG1-S14	747	Jun-03	140	1.0	7.9	18	162	286	2.1
LG1-S11	15	Feb-04	47	3.7	2.8	54	254	179	3.8
LG1-S6	31	Feb-04	66	1.7	0.3	37	109	141	2.1
LG1-S4	61	Feb-04	53	1.0	0.0	15	114	122	2.3
LG1-S1	183	Feb-04	47	4.2	6.6	34	168	136	2.9
LG1-S13	747	Feb-04	140	0.5	30.4	33	162	202	1.4
LG2 site									
LG2-S9	15	Jun-03	95	2.0	1.3	33	169	193	2.0
LG2-S8	31	Jun-03	47	0.7	1.8	19	184	132	2.8
LG2-S6	61	Jun-03	41	0.5	1.0	26	149	165	4.1
LG2-S5	91	Jun-03	38	1.2	0.5	16	169	120	3.2
LG2-S7	122	Jun-03	37	1.7	nd	16	137	125	3.4
LG2-S4	152	Jun-03	28	1.0	nd	20	138	79	2.8
LG2-S3	183	Jun-03	56	1.0	2.0	19	127	120	2.2
LG2-S2	366	Jun-03	66	0.5	3.1	28	220	157	2.4
LG2-S9	15	Feb-04	68	3.0	1.8	45	247	139	2.1
LG2-S8	31	Feb-04	51	0.3	3.1	17	151	139	2.7
LG2-S6	61	Feb-04	40	0.6	-0.2	21	116	100	2.5
LG2-S5	91	Feb-04	36	0.7	1.8	15	127	101	2.8
LG2-S7	122	Feb-04	32	1.3	0.5	13	99	105	3.3
LG2-S4	152	Feb-04	32	1.2	3.0	17	103	94	2.9
LG2-S3	183	Feb-04	50	1.1	2.0	26	117	113	2.3
LG2-S2	366	Feb-04	62	0.5	5.9	29	205	169	2.7
LG3 site									
LG3-S1	61	Feb-04	84	0.5	5.9	23	136	59	0.70
LG3-S5	91	Feb-04	46	1.0	4.3	22	94	120	2.6
LG3-S2	122	Feb-04	34	0.5	nd	27	134	98	2.9
LG3-S7	152	Feb-04	36	1.5	0.3	26	126	125	3.5
LG3-S3	183	Feb-04	60	0.2	2.0	17	126	122	2.0
LG3-S8	213	Feb-04	57	2.7	2.0	20	72	154	2.7
LG3-S9	229	Feb-04	119	4.7	6.4	36	108	252	2.1
Soil paste experiments									
300	2		138	62.9	66.0	41	304	233	1.7
301	6		89	78.3	142.0	244	545	134	1.5
302	10		76	14.5	41.7	94	314	193	2.5
303	15		50	27.9	15.3	13	165	115	2.3
304	20		64	43.9	20.5	33	250	92	1.5
305	25		61	24.2	12.5	17	203	77	1.3
306	35		54	29.4	11.3	16	201	84	1.6
307	45		31	21.2	5.1	10	157	61	2.0
308	55		32	26.4	2.8	11	146	82	2.6
Base/low stream water									
Guaba G1		Jun-03	317	66.6	11.5	42	244	108	0.34
Guaba PRS2		Jun-03	275	63.1	13.3	41	230	104	0.38
Icacos IUP		Jun-03	326	75.8	9.7	48	255	142	0.43

(*continued on next page*)

Table 4 (*continued*)

	Depth (cm)	Sampling date	Si (μmol/kg)	Ca (μmol/kg)	K (μmol/kg)	Mg (μmol/kg)	Na (μmol/kg)	Ge (pmol/kg)	Ge/Si (μmol/mol)
Icacos		Jun-06	258	73.8	15.6	44	204	121	0.47
Icacos		Jun-06	301	80.8	18.7	48	213	120	0.40
Spring water (*landslide scar*)									
LS1		Jun-06	324	60.1	18.4	42	211	105	0.32
LS2		Nov-06	349	63.1	15.3	42	167	109	0.31
LS3		Nov-06	333	61.9	15.9	41	162	96	0.29
LS4		Jun-07	332	66.4	18.9	43	188	89	0.27

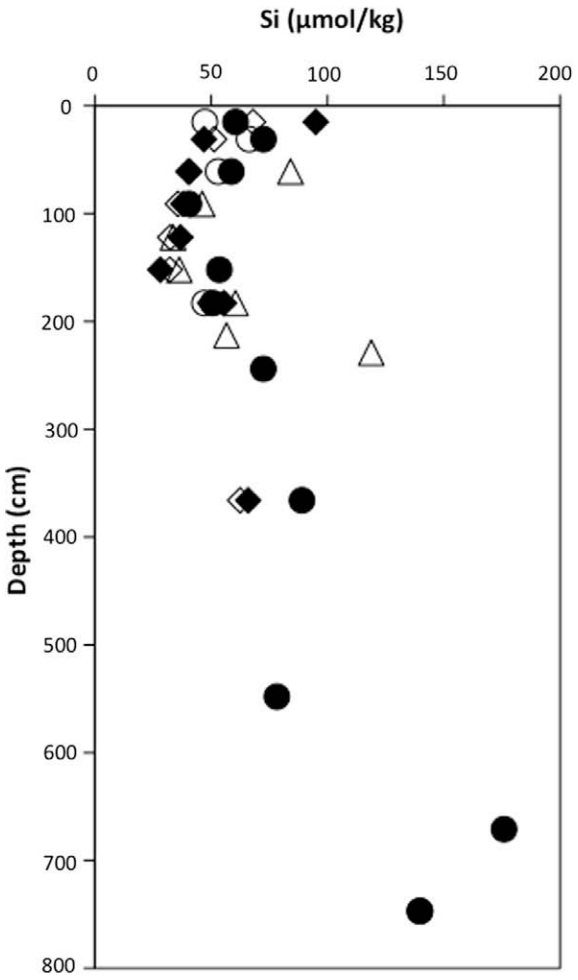

Fig. 4. Pore water Si concentrations from lysimeter samples at LG1, LG2, and LG3. Si concentrations generally decrease upward through the saprolite, then increase again in the shallow soil. Closed symbols are June 2003 samples, open symbols are February 2004 samples. Circles = LG1, diamonds = LG2, triangles = LG3.

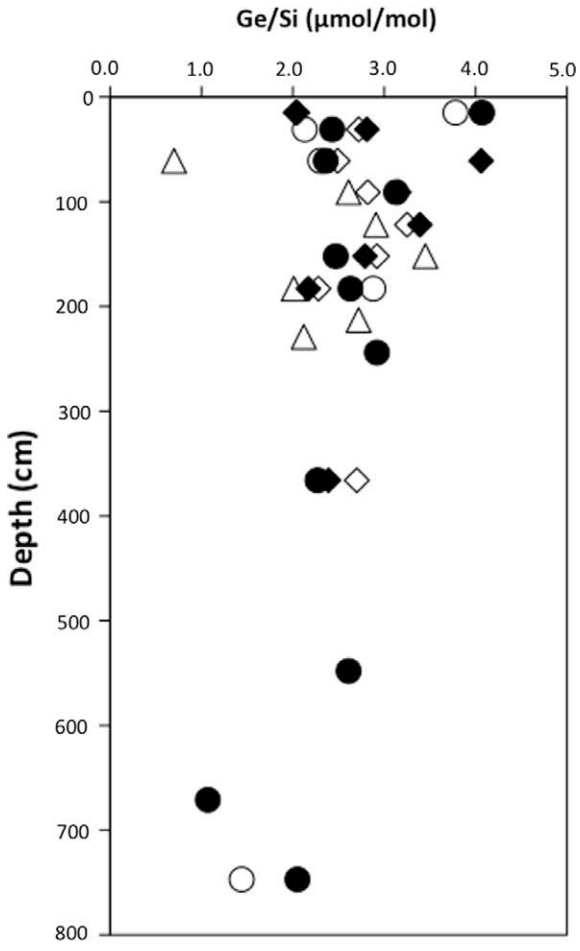

Fig. 5. Pore water Ge/Si ratios from lysimeter samples at LG1, LG2, and LG3. Solute-phase Ge/Si ratios generally increase upward through the saprolite and soil. Symbols same as Fig. 4.

high (or low) Ge/Si ratios. Weathering of the Rio Blanco quartz diorite begins with oxidation of biotite to form "altered biotite". This processes leads to formation and expansion of fractures along which fluids enter bedrock, producing saprock weathering rindlets, and ultimately saprolite (Buss et al., 2008). White et al. (1998) modeled the production of saprolite as incongruent weathering of plagioclase, hornblende, and quartz to form kaolinite. The high Ge/Si ratios of kaolinite (4.8–6.1 μmol/mol) likely reflect preferential incorporation by kaolinite of Ge relative to Si during this process. Although it is difficult to quantitatively account for such high Ge/Si ratios in kaolinite based on the reaction stoichiometry proposed by White et al. (1998; their Fig. 11) and our reactant Ge/Si ratios (Table 1). Soil and saprolite Ge/Si ratios are generally higher than the bedrock ratio at Rio Icacos but we do not observe the extreme Ge/Si fractionation seen in basaltic

weathering profiles (Kurtz et al., 2002; Scribner et al., 2006). Bulk soil and saprolite Ge/Si ratios here most likely reflect the relative amounts of high Ge/Si kaolinite, produced by incongruent weathering of plagioclase and hornblende, and retention of primary igneous quartz, with a low Ge/Si ratio.

Bulk saprolite Ge/Si ratios are roughly constant until about midway up through the saprolite profile. At ~5 m depth, Ge/Si ratios increase to values as high as 3 μmol/mol (Fig. 3). This depth most likely represents the final exhaustion of plagioclase as indicated also by the complete disappearance of Ca (Fig. 2). White et al. (1998) found, in a core sampled near ours, that kaolinite abundance increased from 0% at 8.5 m to about 60% at 5 m. Completion of the transformation of plagioclase to kaolinite explains the high bulk Ge/Si ratios. Within the soil at the top of the weathering profile, Ge/Si ratios decrease sharply (Fig. 3). At this depth, kaolinite produced lower in the saprolite profile is itself being weathered, perhaps due to organic acids in the soil layer increasing the solubility of Al. Decreasing kaolinite abundance in the soil layer is also indicated by the sharp decrease in Al concentrations above 75 cm depth (Table 2). As high Ge/Si kaolinite is lost, bulk soil Ge/Si ratios shift towards the low Ge/Si ratios characteristic of quartz.

5.2. Mass-balance calculations

To better understand the mechanisms of mineral transformations and Ge/Si fractionation in the saprolite and soils, we calculated elemental mass balances using the immobile index element approach. The mass-balance approach is important because changes in elemental concentrations do not accurately reflect loss or gain of elements. Elemental mass balances are calculated relative to an index element assumed to be immobile:

$$\tau_{j,w} = \left(\frac{C_{j,w}}{C_{j,p}} \times \frac{C_{i,p}}{C_{i,w}}\right) - 1 \quad (1)$$

Tau (τ) is the fraction of the mobile element (j) lost from or added to a weathered (soil or saprolite) horizon relative to an immobile element (i), in this case Zr. C is concentration and subscripts w and p represent weathered and parent materials, respectively. Because we cannot show that Zr is conserved (and in fact Zr is sometimes lost during weathering, e.g., Kurtz et al., 2000) the elemental mass balances calculated from Eq. (1) effectively provide lower limits on the loss of mobile elements. Here we will focus on mass balances for Ge, Si, Al, and Ca (Table 5). Positive values of τ indicate gain of a mobile element whereas negative values indicate loss of mobile element. This calculation shows (Table 5) that upwards of 50% of the Si, 70% of the Ge, and 75% of the Al present in the quartz diorite parent material have been lost where weathering is most extensive, in soil within the top 60 cm of the weathering profile.

Values of τ are sensitive to the selected parent material composition, particularly the concentration of the index element. Here we use our measured quartz diorite composition (Table 1). We note that some of the variability in calculated τ values over small changes in depth in Table 5 may be artifacts produced by heterogeneities in the Zr concentration of the original quartz diorite, which is difficult to evaluate, but is likely to be more problematic in plutonic than volcanic rocks. We will therefore focus on elemental mass balances averaged over larger depth zones. Furthermore, given the potential for Zr mobility in tropical weathering profiles (Kurtz et al., 2000) calculated elemental mass balances must be interpreted with some caution.

Table 5
Soil and saprolite Zr-based mass balances calculated relative to bedrock.

Depth (cm)	τ_{Si}	τ_{Ge}	τ_{Al}	τ_{Ca}
15	−0.59	−0.70	−0.77	−1.0
45	−0.45	−0.70	−0.74	−1.0
60	−0.53	−0.62	−0.63	−1.0
75	−0.46	−0.46	−0.38	−1.0
120	−0.44	−0.32	−0.36	−1.0
150	−0.49	−0.26	−0.46	−1.0
180	−0.49	−0.33	−0.38	−1.0
210	−0.42	−0.23	−0.30	−1.0
240	−0.52	−0.42	−0.46	−1.0
270	−0.40	−0.31	−0.36	−1.0
300	−0.57	−0.47	−0.47	−1.0
330	−0.62	−0.65	−0.57	−1.0
360	−0.58	−0.45	−0.54	−1.0
390	−0.42	−0.33	−0.36	−1.0
420	−0.53	−0.29	−0.47	−1.0
450	−0.42	−0.18	−0.31	−1.0
480	−0.65	−0.54	−0.60	−0.96
495	−0.24	−0.20	−0.25	−0.92
510	−0.25	−0.17	−0.24	−0.80
525	−0.56	−0.52	−0.53	−0.88
540	−0.24	−0.24	−0.26	−0.71
555	−0.33	−0.35	−0.31	−0.74
570	−0.33	−0.25	−0.35	−0.59
585	−0.34	−0.33	−0.41	−0.63
600	−0.07	−0.10	−0.13	−0.43
630	−0.30	−0.23	−0.30	−0.55
645	−0.42	−0.47	−0.46	−0.62
660	−0.22	−0.24	−0.28	−0.53
675	−0.44	−0.42	−0.48	−0.62
690	−0.11	−0.03	−0.15	−0.39
705	−0.10	−0.11	−0.17	−0.39
720	−0.39	−0.32	−0.42	−0.56
735	−0.32	−0.27	−0.35	−0.52

With these caveats in mind, here we use the mass-balance approach not only to understand the loss of elements from a particular zone within the weathering profile, but to put constraints on the integrated solution released to stream water in producing that weathered solid residue. For example a τ_{Si} of −0.3 indicates not only that 30% of Si has been lost from bedrock to produce the saprolite, but that the same Si was ultimately exported to stream water. Below we use mass-balance approach to evaluate how weathering losses have dictated the evolution of saprolite and soil Ge/Si ratios, and Ge/Si ratios released to stream water.

Using a value of τ_{Si} calculated from Eq. (1), and measured bulk solid Ge/Si ratios, we can write a mass-balance equation to predict the Ge/Si ratio of the solution derived during weathering of a parent material (bedrock or saprolite) to produce a weathered residue (saprolite or soil):

$$\left(\frac{Ge}{Si}\right)_{solution} = \frac{\left(\frac{Ge}{Si}\right)_{parent} - \left[\left(\frac{Ge}{Si}\right)_{residue}(1+\tau_{Si})\right]}{-\tau_{Si}} \quad (2)$$

We note that the solution composition calculated in this manner is an integrated solution reflecting the change from bedrock to saprolite (or from saprolite to soil). This will not necessarily reflect the solution composition presently measured in soil and saprolite pore waters, both because pore waters are only capturing a snapshot of an ongoing and evolving process, but also because pore waters at depth will reflect a mixture of solutes inherited from their slow movement downward through the profile, perhaps overprinted by re-equilibration with local solids.

5.2.1. Bedrock–saprolite weathering transformation

Weathering of bedrock to saprolite results in significant elemental losses. Taking an average saprolite composition (75–735 cm), we use Eq. (1) to calculate τ values for Si, Ge, and Al of −0.47, −0.39, and −0.44, respectively. In other words development of saprolite results in 47% Si loss, 39% Ge loss, and 44% Al loss from bedrock (Table 6). The preferential retention of Ge by the weathered soil results in an average saprolite Ge/Si ratio of 2.3 μmol/mol. Using Eq. (2), we calculate an integrated solution Ge/Si ratio of 1.7 μmol/mol in the production of saprolite from bedrock (Table 6). This is within range of the values that we find in saprolite pore waters, but significantly higher than ratios measured from baseflow stream chemistry and from spring water (0.27–0.47 μmol/mol), which presumably sample deep weathering reactions. The very low Ge/Si ratios observed in baseflow streams and spring waters may reflect incipient weathering in fractures and saprock weathering rindlets (Buss et al., 2008) where Ge is retained by neoformed kaolinite. Saprolite compositions, even within 50 cm of the saprolite–bedrock interface are Al-depleted, suggesting that some loss of kaolinite in the transformation from saprock to saprolite. Baseflow stream waters compositions apparently reflect this most incipient weathering, and not greatly influenced by the weathering actively taking place within the deep saprolite profile.

5.2.2. Saprolite and soil weathering

Our data allow us to evaluate additional elemental losses as saprolite is further transformed to become soil. We apply the same mass-balance calculations described above, but use the average composition of saprolite (Table 6) as a model parent material for the production of soil. The dramatic decrease in Al concentration from 19.9 to 13.1 (wt% Al_2O_3) is accompanied by a sharp drop in Ge/Si ratio from 2.3 to 1.4 μmol/mol. Our mass-balance calculations (Eq. (1)), now referencing the average soil composition to that of average saprolite, shows that this transformation involves the loss of 18% of Si remaining in saprolite, plus more significant losses of both Ge (50%) and Al (54%). We interpret this as pedogenic dissolution of kaolinite, which hosts much of the remaining Ge and Al, and concentration of residual quartz. Using Eq. (2) to calculate the solution composition released by this transformation, we calculate a solution Ge/Si ratio of 6.4 μmol/mol (Table 6), slightly higher than our average kaolinite Ge/Si ratio. In fact, the solution Ge/Si ratios we find in lysimeter samples from this zone are 2.4–4.1 μmol/mol (Fig. 5), still high, but significantly lower than the value predicted by the mineral mass-balance calculation. Input of silica from labile phytoliths with low Ge/Si could explain the difference between what we predict from the weathering mass balance and what is observed in the soil solution, while also explaining the observed increase in dissolved Si concentrations in soil pore waters relative to underlying saprolite (Fig. 4).

5.3. Phytolith influence in Puerto Rico

Derry et al. (2005) applied the Ge/Si tracer to study Si cycling in Hawaii at the watershed scale and concluded that a biological subcycle has a strong influence on soil water chemistry and stream water Si fluxes in Hawaii. An important question is whether this is a common feature of tropical watersheds or whether Hawaii is a special case. Shallow soil solutions from the Hawaii study generally have Si concentrations >200 μM, with a few up >1500 μM. Ge/Si ratios in these solutions approach the low ratios (~0.1 μmol/mol) measured in phytoliths. In contrast, soil solution Si at the Rio Icacos site never exceeds 200 μM. This does not necessarily mean that there is no role for a biological Si cycle here; plant leaf phytolith contents from the Rio Icacos site (Table 3) are similar to those measured in the Hawaii study. Above we argued that Rio Icacos site soil solution Ge/Si ratios are lower than predicted from mineral mass balance, suggesting a contribution from phytolith dissolution. If the phytolith source has Ge/Si = 0.2 μmol/mol, then derivation of 37–65% of soil solution Si from dissolution of biogenic silica is sufficient to explain the difference between the predicted and observed Ge/Si ratios in the lysimeter samples. Thus a biological subcycle does ap-

Table 6
Stepwise elemental losses during weathering and calculated solution Ge/Si ratio.

	SiO_2 (wt%)	Al_2O_3 (wt%)	CaO (wt%)	Ge (ppm)	Zr (ppm)	Ge/Si solid (μmol/mol)	Weathering step	Si loss (%)	Ge loss (%)	Al loss (%)	Ge/Si solution (μmol/mol)
Average soil (15–60 cm)	77.1	13.1	0.0	1.3	159	1.4	Saprolite → soil	18	50	54	6.4
Average saprolite (75–735 cm)	66.2	19.9	1.9	1.8	112.2	2.3	Bedrock → saprolite	47	39	44	1.7
Rio Blanco quartz diorite	61.8	17.7	6.1	1.5	56	2.0					

pear to influence Si cycling here, but it does not dominate as in Hawaii.

The apparent difference in Si cycling between Hawaii and Puerto Rico must arise from differences in the state factors (e.g., Jenny, 1941) between the two sites, parent material, climate, vegetation type, topography and age. The most obvious difference, and probably the most important in terms of weathering and Si cycling is the parent material, basaltic vs. granitic rocks. The basalt-derived soils of Hawaii evolve towards extreme silica depletion with age (Vitousek et al., 1997; Chadwick et al., 1999). Apart from a steady trickle from Asian dust (Kurtz et al., 2001), there is no new source of Si to the upper soils in Hawaii so biology dominates. Soil solutions take on the low Ge/Si ratios characteristic of phytoliths at Si concentrations approaching opal saturation. The abundant quartz in the granitic parent material at the Rio Icacos site weathers slowly, building a "skeleton" that prevents the extreme volume loss seen in the Hawaiian soils. This quartz is residually enriched in the shallow soils at Rio Icacos, such that bulk soil SiO_2 concentrations reach >80%. Dissolution of kaolinite (along with Saharan dust, Pett-Ridge et al., 2009) appears to supply a steady source of new Si to the biological subcycle.

Climate and microbial activity could also account for differences between Si cycling here and in Hawaii. The Rio Icacos site is both warmer and wetter than the Hawaiian sites studied by Derry et al. (2005). Average temperature at the Hawaii sites is 16 °C vs. 22 °C at the Rio Icacos site. Mean annual precipitation is 250 cm at the Hawaiian sites vs. 420 cm at Rio Icacos. The warm, wet climate contributes to unusually high organic matter decomposition rates (Ostertag et al., 2008). Rapid dissolution of phytolith opal released by decomposing litter might account for the biological contribution to the soil water Si pool proposed above.

5.4. Comparison of silica tracers: Ge/Si vs. δ^{30}Si

Ziegler et al. (2005) studied weathering and silica cycling at the Rio Icacos site from the perspective of Si isotope ratios. Combining their observations with ours provides an excellent opportunity to compare the two tracers. Ziegler et al. demonstrated systematic differences between δ^{30}Si in primary minerals (quartz, plagioclase, biotite), secondary minerals (kaolinite, opal phytoliths) and pore and stream waters. The primary observation, consistent with data from prior studies elsewhere (Douthitt, 1982; De La Rocha et al., 2000; Ding et al., 2004) is that the lighter isotope, ^{28}Si, is preferentially incorporated into secondary minerals such that kaolinite has δ^{30}Si 1.6–2‰ more negative (lighter) than the primary minerals from which it forms. The result of this fractionation is mineral control over pore water δ^{30}Si. Incongruent weathering resulting in precipitation of kaolinite produces isotopically heavy δ^{30}Si in pore water. Deep pore waters and baseflow stream waters have heavier δ^{30}Si than parent materials, reflecting this incongruent weathering source. Ziegler et al. (2005) interpreted an up-profile trend towards lighter pore water δ^{30}Si values as a reflection of additional sources of Si including partial dissolution of quartz, alteration of biotite to kaolinite, and in surface soils, dissolution of isotopically light biogenic opal.

There is a clear and consistent relationship between δ^{30}Si and Ge/Si ratios, both in minerals and especially in pore and stream waters. Dissolved δ^{30}Si and Ge/Si ratios show a strong negative, linear correlation (Fig. 6a), consistent with control by a common mechanism. The relationship between solid-phase δ^{30}Si and Ge/Si ratios (Fig. 6b) is in the same sense, but not as strong. Precipitation of kaolinite preferentially takes up ^{28}Si and Ge, producing a solution with heavy δ^{30}Si and low Ge/Si. Note that this relationship is not consistent with the concept of Ge as a "superheavy stable isotope of Si" (e.g., Azam and Volcani, 1981), because in that case Ge/Si and δ^{30}Si should correlate positively rather than negatively. Ge/Si fractionation may be better treated quantitatively in terms of trace element substitution models (Kurtz et al., 2002) than as an isotope analog.

The difference between the two systems may be best highlighted by the contrasting biological fractionation effects. Plants preferentially incorporate the lighter ^{28}Si isotope in the production of phytoliths (e.g., Ziegler et al., 2005b). This is the same sense of fractionation seen in clays, i.e. both clays and phytoliths have δ^{30}Si lighter than bedrock. The case of Ge/Si is more complicated. While clays preferentially incorporate Ge resulting in high Ge/Si ratios, phytoliths have low Ge/Si ratios, reflecting biological discrimination against Ge (Blecker et al., 2007) or organic sequestration of Ge in plant roots (Delvigne et al., 2009). This contrast may be useful for future studies employing Si tracers to infer the relative roles of weathering and biological cycling on the terrestrial Si cycle.

6. CONCLUSIONS

This study demonstrates the application of Ge/Si ratios as a tracer of Si cycling during weathering in a granitic environment. In a broad sense, the system behaves similarly as previously described for basaltic weathering (Kurtz et al., 2002), where weathering fractionates Ge/Si producing a Ge-enriched residual solid, and low Ge/Si ratios in solution. However, in the granitic parent material studied here, differential weathering rates of primary minerals, each with distinct Ge/Si ratios and associated reaction products strongly influence the Ge/Si ratios of both pore waters and residual bulk solids. We can use these mineral-specific Ge/Si ratios to infer weathering reactions occurring at distinct depth intervals throughout the soil and saprolite profile. The main reaction taking place near the saprolite–bedrock interface involves initial breakdown of plagioclase and hornblende to form Ge-enriched kaolinite. Mass-balance calculations suggest that this process proceeds with 47% Si loss to pore waters, which is ultimately the main source of Si found in springs and streams at baseflow. Later breakdown of kaolinite higher in the weathering profile produces a relatively high Ge/Si ratio, and an additional source of dissolved silica in shallow saprolite and soil solutions.

Although plants in Puerto Rico contain up to 4 wt% SiO_2 as phytoliths, their dissolution does not appear to

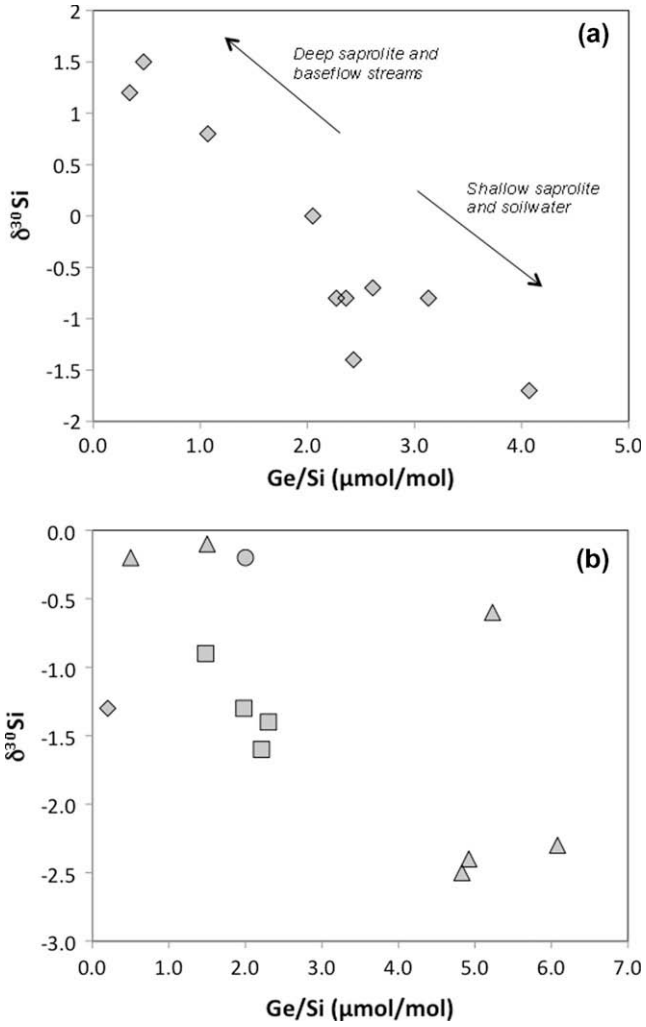

Fig. 6. (a) Pore water and baseflow stream water Ge/Si ratios and δ^{30}Si (data from Ziegler et al., 2005). Samples were collected from the same lysimeters, though not necessarily at the same time. The ratios correlate strongly in a negative sense ($r^2 = 0.87$) suggesting control by common processes. (b) Comparison of solid-phase Ge/Si ratios and δ^{30}Si data (from Ziegler et al., 2005). Circle is quartz diorite bedrock, diamond is average phytolith, squares are bulk saprolite, and triangles are mineral phases (quartz, plagioclase, biotite, kaolinite). The three mineral samples that cluster at low δ^{30}Si are kaolinite.

dominate shallow soil pore waters to the extent that has been shown for Hawaii (Derry et al., 2005). Still, our mass-balance calculations suggest that perhaps 50% of dissolved Si in shallow soils may be cycled through a biological pool, so the effect of plants on shallow soil pore water compositions is not negligible. In Hawaii, Ge/Si ratios show that biological cycling and phytolith dissolution strongly influence stream water Ge/Si ratios and Si concentrations (Derry et al., 2005). Ge/Si ratios here clearly show that baseflow stream waters at Rio Icacos are controlled by deep weathering reactions and not by a shallow biological overprint.

ACKNOWLEDGMENTS

We thank Joe Troester, Jamie Shanley, Manuel Rosaria, Heather Buss, Julie Pett-Ridge, Tony Hartshorn and Cary Kandel for their help in the field. Comments from Flip Froelich and an anonymous reviewer improved the original manuscript. This work was funded by NSF Grants EAR-0208336 and EAR-0538127.

REFERENCES

Anders A. M., Sletten R. S., Derry L. A. and Hallet B. (2003) Germanium/silicon ratios in the Copper River Basin, Alaska: weathering and partitioning in periglacial versus glacial environments. *J. Geophys. Res.* **108**. doi:10.1029/2003JF000026.

Anderson S. P., Dietrich W. E. and Brimhall G. H. (2002) Weathering profiles, mass-balance analysis, and rates of solute loss: linkages between weathering and erosion in a small, steep catchment. *Geol. Soc. Am. Bull.* **114**, 1143–1158.

Azam F. and Volcani B. E. (1981) Germanium–silicon interactions in biological systems. In *Silicon and Siliceous Structures in Biological Systems* (eds. T. L. Simpson and B. E. Volcani). Springer-Verlag, New York.

Bernstein L. R. (1985) Germanium geochemistry and mineralogy. *Geochim. Cosmochim. Acta* **49**, 2409–2422.

Blecker S. W., King S. L., Derry L. A., Chadwick O. A., Ippolito J. A. and Kelly E. F. (2007) The ratio of germanium to silicon in plant phytoliths: quantification of biological discrimination under controlled experimental conditions. *Biogeochemistry* **86**, 189–199.

Blum J. D., Erel Y. and Brown K. (1993) Sr-87/Sr-86 ratios of Sierra-Nevada stream waters – implications for relative mineral weathering rates. *Geochim. Cosmochim. Acta* **57**, 5019–5025.

Boccheciamp R. A. (1977) Soil survey of Humacao area of eastern Puerto Rico. United States Department of Agriculture, Soil Conservation Service.

Brown S., Lugo A. E., Silander S. and Liegel L. (1983) Research history and opportunity in the Luquillo Experimental Forest. *USDA General Technical Report*.

Buss H. L., Sak P. B., Webb S. M. and Brantley S. L. (2008) Weathering of the Rio Blanco quartz diorite, Luquillo Mountains, Puerto Rico: coupling oxidation, dissolution, and fracturing. *Geochim. Cosmochim. Acta* **72**, 4488–4507.

Capo R. C., Stewart B. W. and Chadwick O. A. (1998) Strontium isotopes as tracers of ecosystem processes: theory and methods. *Geoderma* **82**, 197–225.

Chadwick O. A., Derry L. A., Vitousek P. M., Huebert B. J. and Hedin L. O. (1999) Changing sources of nutrients during four million years of ecosystem development. *Nature* **397**, 491–497.

Day P. R. (1965) Method for separation of clay, silt and sand fractions. In *Methods of Soil Analysis. Part 1: Physical and Mineralogical Properties, Including Statistics of Measurement and Sampling* (eds. C. A. Black, D. D. Evans, L. E. White, F. E. Ensminger and F. E. Clark). Soil Science Society of America, Madison, WI.

DeArgollo R. and Schilling J.-G. (1978) Ge–Si and Ga–Al fractionation in Hawaiian volcanic rocks. *Geochem. Cosmochem. Acta* **42**, 623–630.

De La Rocha C. L., Brzezinski M. A. and DeNiro M. J. (2000) A first look at the distribution of the stable isotopes of silicon in natural waters. *Geochim. Cosmochim. Acta* **64**, 2467–2477.

Delvigne C., Opfergelt S., Cardinal D., Delvaux B. and Andre L. (2009) Distinct silicon and germanium pathways in the soil-plant system: evidence from banana and horsetail. *J. Geophys. Res. – Biogeosci.* **114**, G02013.

Derry L. A., Kurtz A. C., Ziegler K. and Chadwick O. A. (2005) Biological control of terrestrial silica cycling and export fluxes to watersheds. *Nature* **433**, 728–731.

Derry L. A., Pett-Ridge J. C., Kurtz A. C. and Troester J. W. (2006) Ge/Si and Sr-87/Sr-86 tracers of weathering reactions and hydrologic pathways in a tropical granitoid system. *J. Geochem. Exploration* **88**, 271–274.

Ding T., Wan D., Wang C. and Zhang F. (2004) Silicon isotope compositions of dissolved silicon and suspended matter in the Yangtze River, China. *Geochim. Cosmochim. Acta* **68**, 205–216.

Dong H. L., Peacor D. R. and Murphy S. F. (1998) TEM study of progressive alteration of igneous biotite to kaolinite throughout a weathered soil profile. *Geochim. Cosmochim. Acta* **62**, 1881–1887.

Douthitt C. B. (1982) The geochemistry of the stable isotopes of silicon. *Geochim. Cosmochim. Acta* **46**, 1449–1458.

Froelich P. N., Blanc V., Mortlock R. A., Chillrud S. N., Dunstan W., Udomkit A. and Peng T.-H. (1992) River fluxes of dissolved silica to the ocean were higher during the glacials: Ge/Si in diatoms, rivers, and oceans. *Paleoceanography* **7**, 739–768.

Gaillardet J., Dupre B., Louvat P. and Allegre C. J. (1999) Global silicate weathering and CO_2 consumption rates deduced from the chemistry of large rivers. *Chem. Geol.* **159**, 3–30.

Garrels R. M. and Mackenzie F. T. (1967). *Origin of the chemical compositions of some springs and lakes*. .

Goldschmidt V. M. (1926) Über das Krystallochemische und geochemische Verhalten des Germaniums. *Naturewissenschaften* **14**, 295–297.

Goldschmidt V. M. (1958) Geochemistry. Oxford University Press, London.

Jenny H. (1941) Factors of Soil Formation. McGraw-Hill Book Co., New York.

Jin K., Shibata Y. and Morita M. (1991) Determination of germanium species by hydride generation-inductively coupled plasma mass spectrometry. *Anal. Chem.* **63**, 986–989.

Kurtz A. C., Derry L. A., Chadwick O. A. and Alfano M. J. (2000) Refractory element mobility in volcanic soils. *Geology* **28**, 683–686.

Kurtz A. C., Derry L. A. and Chadwick O. A. (2001) Accretion of Asian dust to Hawaiian soils: isotopic, elemental, and mineral mass balances. *Geochim. Cosmochim. Acta* **65**, 1971–1983.

Kurtz A. C., Derry L. A. and Chadwick O. A. (2002) Germanium–silicon fractionation in the weathering environment. *Geochim. Cosmochim. Acta* **66**, 1525–1537.

Lathja K., Jarrell W. M., Johnson D. W. and Sollins P. (1999) Collection of soil solution. In *Standard Soil Methods for Long-term Ecological Research* (eds. G. P. Robertson, D. C. Coleman, C. S. Bledsoe and P. Sollins). Oxford University Press, New York.

Lewis B. L., Andreae M. O., Froelich P. N. and Mortlock R. A. (1988) A review of the biogeochemistry of germanium in natural waters. *Sci. Total Environ.* **73**, 107–120.

Martin F., Ildefonse P., Hazemann J.-L., Petit S., Grauby O. and Decarreau A. (1996) Random distribution of Ge and Si in synthetic talc: an EXAFS and FTIR study. *Eur. J. Mineral.* **8**, 289–299.

Mcdowell W. H. and Asbury C. E. (1994) Export of carbon, nitrogen, and major ions from 3 Tropical Montane Watersheds. *Limnol. Oceanogr.* **39**, 111–125.

Mortlock R. A. and Froelich P. N. (1987) Continental weathering of germanium: Ge/Si in the global river discharge. *Geochem. Cosmochem. Acta* **51**, 2075–2082.

Mortlock R. A. and Froelich P. N. (1996) Determination of germanium by isotope dilution-hydride generation inductively coupled plasma mass spectrometry. *Anal. Chem. Acta* **332**, 277–284.

Murnane R. J. and Stallard R. F. (1990) Germanium and silicon in rivers of the Orinoco drainage basin. *Nature* **344**, 749–752.

Murphy S. F., Brantley S. L., Blum A. E., White A. F. and Dong H. (1998) Chemical weathering in a tropical watershed, Luquillo Mountains, Puerto Rico. II. Rate and mechanism of biotite weathering. *Geochim. Cosmochim. Acta* **62**, 227–243.

Ostertag R., Marin-Spiotta E., Silver W. L. and Schulten J. (2008) Litterfall and decomposition in relation to soil carbon pools along a secondary forest chronosequence in Puerto Rico. *Ecosystems* **11**, 701–714.

Pett-Ridge J. C., Derry L. A. and Kurtz A. C. (2009) Sr isotopes as a tracer of weathering processes and dust inputs in a tropical granitoid watershed, Luquillo Mountains, Puerto Rico. *Geochim. Cosmochim. Acta* **73**, 25–43.

Scribner A. M., Kurtz A. C. and Chadwick O. A. (2006) Germanium sequestration by soil: targeting the roles of secondary clays and Fe-oxyhydroxides. *Earth Planet Sci. Lett.* **243**, 760–770.

Seiders V. M. (1971). *Geologic map of the El Yunque quadrangle, Puerto Rico*. .

Shannon R. D. (1976) Revised effective ionic-radii and systematic studies of interatomic distances in halides and chalcogenides. *Acta Crystallogr. A* **32**, 751–767.

Shannon R. D. and Prewitt C. T. (1969) Effective ionic radii in oxides and fluorides. *Acta Crystallogr. B* **25**, 925–946.

Stonestrom D. A., White A. F. and Akstin K. C. (1998) Determining rates of chemical weathering in soils – solute transport versus profile evolution. *J. Hydrol.* **209**, 331–345.

Turner B. F., Stallard R. F. and Brantley S. L. (2003) Investigation of in situ weathering of quartz diorite bedrock in the Rio Icacos basin, Luquillo Experimental Forest, Puerto Rico. *Chem. Geol.* **202**, 313–341.

Vitousek P. M., Chadwick O. A., Crews T. E., Fownes J. H., Hendricks D. M. and Herbert D. (1997) Soil and ecosystem development across the Hawaiian Islands. *GSA Today* **7**, 1–8.

White A. F., Blum A. E., Schulz M. S., Vivit D. V., Stonestrom D. A., Larsen M. and Murphy S. F. (1998) Chemical weathering in a tropical watershed, Luquillo Mountains, Puerto Rico. I. Regolith weathering rates. *Geochim. Cosmochim. Acta* **62**, 209–226.

Ziegler K., Chadwick O. A., White A. F. and Brzezinski M. A. (2005a) (DSi)-Si-30 systematics in a granitic saprolite, Puerto Rico. *Geology* **33**, 817–820.

Ziegler K., Chadwick O. A., Brzezinski M. A. and Kelly E. F. (2005b) Natural variations of delta Si-30 ratios during progressive basalt weathering, Hawaiian Islands. *Geochim. Cosmochim. Acta* **69**, 4597–4610.

Associate editor: Jon Chorover